

Doubly Stochastic Earthquake Source Model: “Omega-Square” Spectrum and Low High-Frequency Directivity Revealed by Numerical Experiments

A. A. GUSEV^{1,2}

Abstract—Since its formulation in 1967–1970, the classical ω^{-2} model of earthquake source spectrum awaits a consistent theoretical foundation. To obtain one, stochastic elements are incorporated both into the final structure of the fault and into the mode of rupture propagation. The main components of the proposed “doubly stochastic” model are: (1) the Andrews’s concept, that local stress drop over a fault is a random self-similar field; (2) the concept of rupture with running slip pulse, after Heaton; (3) the hypothesis that a rupture front is a tortuous, multiply connected (“lacy”) fractal polyline that occupies a strip of finite width close to the slip-pulse width; and (4) the assumption that the propagation distance of fault-guided, mostly Rayleigh waves from a failing spot on a fault is determined by the slip-pulse width. Waveforms produced by this model are determined based on the fault asperity failure model after Das and Kostrov. Properties of the model are studied by numerical experiments. At high frequency, simulated source spectra behave as ω^{-2} , and acceleration spectra are flat. Their level, at a given seismic moment and rms stress drop, is inversely related to the relative width of the slip pulse. When this width is relatively low, a well-defined second corner frequency (lower cutoff of acceleration spectrum) is seen. The model shows clear dependence of propagation-related directivity on frequency. Between the first and the second corner frequency, amplitude spectra are strongly enhanced for the forward direction; whereas, above the second corner frequency, directivity is significantly reduced. Still, it is not inhibited totally, suggesting incomplete incoherence of the simulated radiator at high frequencies.

Key words: Self-similar, random, stress drop field, fractal, acceleration, slip pulse, random rupture front, frequency-dependent directivity.

1. List of denotations and abbreviations

The following three earthquake source models will be discussed: Case F1: asperity-source on an infinite planar fault P with zero cohesion (DAS and KOSTROV 1983, henceforth referred to as DK83); Case F2: fault-source P of finite area that contains single smaller-size asperity and whose cohesion equals zero over the rest of its surface (DAS and KOSTROV 1986; henceforth referred to as DK86); and Case F3: finite fault-source P whose entire area is a composition of spots/asperities of finite or infinitesimally small area (DAS and KOSTROV 1988, henceforth referred to as DK88; BOATWRIGHT 1988, henceforth referred to as B88; GUSEV 1988, henceforth referred to as G88; GUSEV 1989). The superscript “ ∞ ” is used for Case F1 where appropriate.

$\mathbf{x} = \{x, y, z\}$	Cartesian coordinates of the receiver point; selected so that $z = 0$ on a planar fault P
$\xi = \{\xi_1, \xi_2, 0\}$	Cartesian coordinates of a radiating point on P
Σ_a	Asperity area in Cases F1 and F2; located on P
$2R_a$	Its characteristic size (e.g. diameter)
Σ	Entire source area in Cases F2 and F3, located on P
$2R_c$	Its characteristic size. For Case F2, $R_c \gg R_a$. It is assumed that fault length $L \approx 2R_c$
dS	Infinitesimally small element of Σ_a or of Σ
ΔS	Small element of Σ in Case F3, of size $\Delta S^{0.5}$. A generalization of a single asperity treated in Cases F1 and F2, of size $2R_a$

¹ Institute of Volcanology and Seismology, Russian Ac. Sci, 9 Piip Blvd, Petropavlovsk-Kamchatsky 683006, Russia. E-mail: gusev@emsd.ru

² Kamchatka Branch, Geophysical Service, Russian Ac. Sci, 9 Piip Blvd, Petropavlovsk-Kamchatsky 683006, Russia.

R_s	<p>Characteristic propagation distance of inhomogeneous waves (Rayleigh and other) guided by the free fault surface. These waves are generated by asperity failure in Cases F1 and F2, and by each ΔS in Case F3. Called “slip radius” in B88. In Case F2, $R_s = R_c$. At distances close to R_s, inhomogeneous fault-guided waves die off and do not propagate farther</p>	R	<p>Hypocenter-to-receiver distance, it is assumed that $R \gg R_a$ and $R \gg R_c$</p>
		$F_0 = \int_{\Sigma_a} \tau(\xi) dS$	<p>Seismic force of an asperity source; introduced in DK83 for Case F1; still meaningful for Case F2. Valid for the Case F3 when the area of integration is replaced by Σ</p>
c_S	<p>S-wave velocity</p>	f_{c1}	<p>Common (leftmost) corner frequency, crossover point where theoretical or empirical source spectrum trend turns from f^0 to f^{-2}, f^{-1} or, generally f^γ. A model-independent definition of f_{c1} is used here based on log-spectrum expansion into MacLaurin series (SILVER 1983); f_{c1} is defined as $1/2\pi T_{rms}^2$, where T_{rms}^2 is the second normalized central power moment for a displacement waveform</p>
v	<p>Mean velocity of rupture front; it is assumed to be close to c_S</p>		<p>Second from the left corner frequency, crossover point where source spectrum trend turns from (accurately or approximately) f^{-1} to f^{-2}; simultaneously: left cutoff of approximately flat source acceleration spectrum. May coincide with f_{c1}; this case is one of the “ω^{-2}” spectral model</p>
$T_a \approx 2R_a/c_S$ $\approx 2R_a/v$	<p>Characteristic duration of rupture propagation over in Cases F1 and F2</p>	f_{c2}	<p>Frequency of transition between ranges of high and low directivity; these cases are understood as the manifestations of, respectively, effectively coherent and effectively incoherent space-time organization of the radiating fault; the denotation means “upper bound of coherent behavior”. Introduced in (GUSEV 2013a).</p>
$T_c \approx (1 - 2)R_c/c_S$ $\approx (1 - 2)R_c/v$	<p>Characteristic duration of rupture process in Cases F2 and F3</p>		<p>Is close to $1/T_0$ as defined by BERNARD and HERRERO (1994)</p>
$T_s \approx R_s/c_S$	<p>Characteristic time associated with R_s</p>	f_{ucoh}	
$\tau(\xi)$	<p>Local dynamic stress drop on dS; it is assumed that $\tau(\xi) > 0$</p> <p>In time, this stress drop is assumed to occur abruptly: its time history $\tau(\xi, t) \equiv \tau(\xi)H(t)$ where $H(t)$ is the Heaviside step</p>		
T_r	<p>Rise time, defined as twice the centroid of slip rate time history at ξ. It is assumed that $T_s \approx T_r$</p>		
L	<p>Width of running slip pulse</p> <p>$l = vT_r$</p>		
C_H	<p>Haskell–Heaton constant; $C_H = l/L$. In the case when T_r and l vary over a fault, C_H is understood as the average value over fault area</p>		
w	<p>Characteristic width of the “thick” lacy random rupture front or “front strip”. It is assumed here to coincide with l</p>		
T_w	<p>Temporal width of the “front strip”; $T_w = w/v$</p>		

$f_{c1,90}, f_{c2,90}$	The values of f_{c1} and f_{c2} for the ray normal to the fault
$t_{fr}(\xi)$	Is the time of arrival of rupture front to ξ ; it is simulated numerically as the sum of three terms: deterministic low-wavenumber term $Q_{det}(\xi)$ that describes systematic propagation of the front, random high-wavenumber term $Q_{rnd}(\xi)$ that describes fine details of the front geometry, and random low-wavenumber term $Q_{lk}(\xi)$ that perturbs $Q_{det}(\xi)$, of secondary importance
CCM	Composite-crack source model: a source consists of a number of isolated slip patches or cracks abutting one another; proposed by BOATWRIGHT (1982) and PAPAGEORGIOU and AKI (1983)
SPM	Slip-pulse source model; proposed and substantiated by HEATON (1990) who developed the concept of HASKELL (1964)

ω^{-1} branch. This behavior of “ $\omega^0-\omega^{-1}-\omega^{-2}$ ” needs two corner frequencies: f_{c1} , and $f_{c2} > f_{c1}$. BRUNE (1970) associated the emergence of the second corner with the fractional stress drop over a fault. GUSEV (1983) noted that spectral shapes with the second characteristic frequency clearly above f_{c1} are ubiquitous for moderate-to-large magnitudes; in essence, he provided empirical support for the idea of a two-corner spectrum. Since then, this guess was reliably confirmed further by analyses of many studied data sets; see GUSEV (2013a) for a fresh review on f_{c2} . HANKS and MCGUIRE (1981) found that the flat acceleration spectrum of BRUNE’S (1970) ω^{-2} model fits well the smoothed observed spectra of strong motion. In essence, they treated the deterministic spectra of BRUNE (1970) as rms spectra of a certain, implicitly introduced, stochastic model, and with great success. ANDREWS (1980) proposed to treat the final slip over a fault as a random self-affine function, whose 2D Fourier spectrum is asymptotically of the $1/k^\alpha$ type. He also has shown that the field of local stress drop has a spectrum of a similar ($1/k^\beta$) kind. ANDREWS (1980) also suggested that real faults are not only self-affine, but self-similar; in this case, $\alpha = 2$ and $\beta = 1$. Inverted slip distributions over real faults generally support this idea (TSAI 1997, SOMERVILLE *et al.* 1999) despite certain deviations. BERNARD and HERRERO (1994; see also HERRERO and BERNARD 1994) noticed that the instant dislocation jump that propagates over Andrews’ fault with $\alpha = 2$ generates random signal with ω^2 spectrum. In general, the idea to explain ω^2 spectra through spatial spectra of fault heterogeneity looks attractive.

2. Introduction

The first stochastic model of an earthquake fault is one proposed by HASKELL (1966), who modified his running dislocation model (HASKELL, 1964) by introducing a random local dislocation (slip) rate. This space-time function was specified through its correlation functions: in time (1D) and in space (2D). AKI (1967) modified Haskell’s correlation function to make displacement spectra of radiated body waves to behave as ω^{-2} at high frequencies (HF), instead of the less realistic ω^{-3} of HASKELL’S (1966) model. BRUNE (1970) reduced this concept to a simpler, deterministic, one. The best-known part of his theory treats the simple one-corner ω^{-2} spectral model, with a single corner frequency denoted here as f_{c1} . He also noted, however, that a more realistic spectral model of the general ω^{-2} kind may need an intermediate

Two-corner spectra represent a characteristic property of multiple-subsource, composite-crack source models (CCM) (PAPAGEORGIOU and AKI 1983). Both in general, and in CCM in particular, the lower corner f_{c1} is close to inverse rupture duration, whereas the second, upper corner f_{c2} of CCM is related to the duration of a subsource. Although the assumption of ubiquitous isolated subsources of CCM raises doubts from a tectonophysical viewpoint (GUSEV 1983, 2013a), CCM constitutes a rather successful scheme for practical numerical modeling of HF radiation (BERESNEV and ATKINSON 2002; HALLDORSSON and PAPAGEORGIOU 2005). Thus, any competing source model should operate not worse

than CCM. In CCM, local stress drop (i.e. average over a subsource) is many times above the average/global stress drop over an entire composite fault. Taking local stress drop as a reference value, the CCM can be classified as one with fractional stress drop as introduced by BRUNE (1970).

Another concept of rupture evolution that also features fractional stress drop, is the slip-pulse model (SPM) (HEATON 1990), which inherited important features of HASKELL (1964, 1966). Different from CCM, this model does not assume any unbreakable barriers: slip pulse sweeps the entire fault. Such a behavior is much more plausible tectonophysically. Each of the two models—CCM and SPM—contains a dimensionless parameter of scale ratio, namely, for SPM, the running strip width l to source length L ratio, l/L , in the 0.025–0.15 range (HEATON 1990), and, for CCM, the subsource/composite source size ratio of comparable magnitude. In both cases, such a ratio gives a rough estimate of the ratio of mean global stress drop to local stress drop, thus describing numerically the fractional character of stress drop. The value of l is proportional to rise time T_r of dislocation.

Let us consider HF fault radiation, i.e. radiation in the frequency range well above f_{c1} . Its important property is low directivity. Weak HF directivity is a well-expressed feature, clearly manifest as the typical lack of expressed asymmetry for isoseismal maps (and for peak acceleration maps) around a finite surface-focus earthquake source of moderate-to-large magnitude, even for clearly unilateral ruptures; see examples in GUSEV (2013a). This feature is seen best for the two highest isoseismals. There are other causes for asymmetric isoseismals: radiation pattern of a point source, non-uniform attenuation, as well as uneven site effects. All these make various imprints on isoseismal pattern, but none among them might be capable of suppressing a specific pattern expected for deterministic unilateral ruptures, with an expressed unilateral lobe, specific for the discussed kind of directivity (see e.g. BOATWRIGHT 1982). As for frequency-dependent directivity of HF amplitudes, see TSAI (1997), SOMERVILLE (1997) for deeper analysis. For deterministic fault rupture models, both of a dislocation or of crack kind, one can expect expressed directivity; thus, the property that needs theoretical

explanation is, rather, significant diminution of directivity at HF. The probable cause of low HF directivity is the incoherence of HF radiation (KOSTROV 1975; BOATWRIGHT 1982; GUSEV 1983). From the observational viewpoint, incoherence is suggested by a noise-like appearance of HF records, and conceptually it can be associated with random phases of waveforms contributed by elemental spots of a fault. Randomness of phases is a key factor that underpins the application of rms amplitudes (and, essentially, energy spectra) in strong motion analyses at HF, e.g. in HANKS and MCGUIRE (1981). For lower frequencies (typically below 0.5–1 Hz), however, directivity becomes quite noticeable; near the source it shows itself particularly clearly as the emergence of “forward-directivity pulses” (SOMERVILLE 1997). For smaller magnitudes, directivity is clearly manifest at high frequencies (BOATWRIGHT 2007) if one defines “high frequency” in absolute terms, as this is commonly done; but for smaller events, this part of the spectrum seems to be associated with coherent radiation, and thus shows clear directivity. Thus, the presence of directivity at low magnitude seems to be an apparent problem that calls for a physically consistent, non-dimensional definition of “high frequency”. See more on this point in (GUSEV 2013a). BERNARD and HERRERO (1994) associated the transition point from higher low-frequency directivity to diminished HF directivity with characteristic frequency $1/T_0$ associated with rise time: $T_0 \approx T_r$. This guess is generally confirmed below.

As a different cause of diminution of directivity effects (as well as radiation pattern ones), one may imagine wave scattering, usually expressed just at HF. Simulation suggests, however (GUSEV and ABYBAKIROV 1996), that significant randomization of radiation pattern and/or directivity by scattering may be expected only at the “diffusion mode” scattering. This mode appears at lapse times on the order of $3 \times$ (transport mean free path TMFP)/(wave speed c_s) or later. At values TMFP = 50–100 km and $c_s = 3.5$ km/s, typical for regional distances, this means delays like $150\text{--}300/3.5 = 40\text{--}90$ s. This is much above typical direct wave travel time for waveforms that produce strong motion/isoseismal data. At more relevant travel times like 10–30 s, scattering is mostly of the “forward” kind (preferably

at small angle relative to the ray direction). Directivity is only slightly suppressed in this case (whereas nodal-plane holes in the radiation pattern may be significantly smoothed over).

The three listed features— ω^{-2} HF spectral asymptote, two-corner spectral shape of, roughly, the ω^0 – ω^{-1} – ω^{-2} kind, and expressed frequency dependence of directivity—all lack systematic theoretical explanation. Textbooks (e.g. SHEARER 1999), illustrate spectral features by source time function (STF) that is a convolution of two boxcars, whose widths are defined by (1) rupture propagation duration, and (2) rise time of local slip. In general terms, the imprint of these two characteristic times on spectral shapes in the form of two corresponding corner frequencies is a quite reasonable idea, and it is completely supported by the present study. However, in the time domain, convolution of the two boxcars creates the deterministic displacement STF of trapezoidal shape, and, therefore, unrealistic far-field accelerogram that consists of exactly four delta-functions and nothing else. An attempt to iron out this problem by smoothing of any of the two unrealistically sharp boxcar shapes immediately leads to significantly faster spectral decay as compared to the ω^{-2} kind. Thus, such a description of STF is oversimplified. More realistic model of STF is needed, such that might preserve two-corner spectra with ω^{-2} overall behavior, and, simultaneously, show realistic, white-noise style, acceleration waveform. Note that CCMs generate two-corner spectra, but the rise time concept is alien to these models. As for low HF directivity, although its connection with the incoherency property of a HF source has been suggested in general terms, there is no model that would reproduce this property in a conceptually consistent way. The CCM does show incoherency (formed by randomly perturbed timing of subsources) but these “subsources” seem to be an artificial construct. At any rate, an appropriate model that might explain the mentioned properties must probably be of a stochastic kind. To propose a model of this type is the key intention of the present paper.

Fault description developed here is based on local stress drop, and differs from the common approach based on local slip rate. The general idea to represent radiated earthquake waves as a sum of contributions of fault spots characterized by their stress drops was

introduced in parallel, but from non-identical view-points in DK88, in B88 (“composite asperity model”) and in G88. (The last paper is in Russian; the paper in English, GUSEV (1989), covers similar points and is easier to access; only the earlier paper will be referred to in the following). DK88 and G88 considered only strong spots (small asperities) dotted over background of negligible strength; whereas B88 considered all fault spots. In DK88, a number of multiple-asperity example faults are accurately simulated deterministically, whereas both G88 and B88 analyzed a multitude of asperities in less detail and in a stochastic manner. In particular, they assumed pulses from asperities to add incoherently at high frequency. G88 also discussed the structure of the rupture front and treated it as a “wave of breaking of asperities”, i.e. a loosely organized feature, resulting in randomly phased contribution of asperity-generated pulses at a receiver. The present work elaborates on these concepts.

The main idea here is to combine two separate stochastic models. One of them is purely spatial and describes the fields of final slip and of local stress drop over a fault as random functions, following ANDREWS (1980). Another model describes fault evolution in space–time: this evolution is represented by a propagating rupture front whose instant geometry is a wiggling, multiply connected (“lacy”) random polyline of fractal type (GUSEV 2013a), instead of a commonly assumed smooth curve. This random polyline is thought to be “thick”: at any time instant, it occupies a strip with loosely defined margins, but of finite width w . This polylinear geometrical object will be called “front strip.” The combination of these two models will be called “doubly stochastic source model”. Other significant components of the present approach are: the notion of running slip-pulse rupture (HEATON 1990), whose width l is thought to be close to w ; and application of the fault asperity failure model of DK83 and DK86 that permits one to relate formation of the complete earthquake wavetrain to fault failure and to propagation of fault-guided (mostly Rayleigh) waves over the non-locked part of a fault. The last critical assumption made here following B88 and G88 is that an arbitrary failing spot on a fault can be treated as an asperity that generates fault-guided waves that travel a certain distance along the non-

locked part of the fault. However, in contrast to B88 and G88, this value is thought here to be close to l and w . (The fault-guided waves discussed here are strictly confined within the slipping part of the source-fault, and should not be confused with regular guided waves that may propagate in a fault-related low-velocity waveguide.)

The set of described assumptions was implemented as a simulation code based on a simplified kinematic description of rupture evolution. The properties of the doubly stochastic source model are studied through numerical experiments. In these, all the three above-mentioned empirical properties of fault-generated radiation are manifest. The results may provide a solution for an old puzzle, and are also important for applications.

A preliminary, highly compressed version of a part of the results presented here was recently published in GUSEV (2013b).

3. General Background

As an elastodynamical basis of the present approach, the fault asperity concept after Das and Kostrov is employed. They analyzed, in DK83, radiation generated by failure of a strong patch—an asperity—on an infinite fault which is weak, i.e. with negligible cohesion (Case F1). They considered this analysis as a first step in understanding seismic waves radiated by real faults with their widely varying strength. In the next step in DK86, they modified their results for the case of a similar single asperity on a *finite* weak fault (Case F2). Lastly, in DK88 they analyzed a weak fault with multiple asperities. To understand better their way of treatment of fault radiation one should realize that it is somewhat unusual. Generally, there are two equivalent ways to represent the source of elastic radiation field of a fault: via double-couple density—the common one, and via stress change/drop. Despite similarity of appearance of corresponding integrals, there are significant differences. In the double-couple description, no fault dislocation exists: a fault with dislocations is *represented* by double-couples inserted into homogeneous medium whose cut is welded. This representation, in addition to its many positive points,

has some inconveniences. One cannot determine dislocations and their rates while stepping in time (because of point-to-point interaction). On the contrary, the use of stress change permits direct integration in time along the rupture front, and thus presents some advantage. But only in the case of infinite fault is it a relatively easy procedure. In this case, there are two contacting halfspaces, and in each halfspace, the asperity failure is equivalent to the switching on of a force spread over the asperity area. The forces in the two halfspaces are equal and of opposite sign. Body wave displacement time history from such a failure represents a smoothed step at any distance, including far field. The case of finite fault was analyzed numerically in DK86 and DK88; of course, no static step for the far field appears in these cases (although numerical integration in DK88 cannot show this with full clarity). Use of stress-change description of finite fault evolution is the key point of the present paper. However, the presentation below begins with the introductory Case F1 of infinite fault.

A remarkable feature of the DK86 model (F2) is the emergence of two balanced forces applied to the opposite walls of the finite weak fault, i.e. of the cut in the elastic space. Just these forces generate initial parts of body waveforms that are essentially static far field displacements. These displacements persist until fault-guided, mostly Rayleigh, waves reach the boundary of the fault and in their diffraction, create backward static displacement that precisely compensates the first one; consequently, the summary static offset equals zero. Fault-guided waves are a strictly transient phenomenon; it accompanies formation of the free surface of the cut that arises temporarily during rupture evolution.

The approach of DK83 and DK86 was developed in DK88, and, on a less strict level, in B88 and G88, who tried to apply it to observable entities. Analysis in B88 is concentrated on spectral description of the radiator. It is noted in B88 that one can treat the fault radiation as a combination of contributions of fault spots/asperities covering the entire fault surface. Therefore, the usage of the term “asperity” in B88 is somewhat loose and a large fraction of these “asperities” could only be relatively weak. For the present paper, it is important to note that the analysis of B88 is applicable for any decomposition of the entire fault

into “asperities”, in particular into the great number of small ones.

In G88, both spectral and time-domain features are analyzed. It is supposed that significant contribution into strong motion comes from strongest fault patches, and the role of the remaining part of fault area (taken as 90–95 %) can be neglected. Rupture evolution was thought to be a “wave” of the switching on of asperities, with some average tendency that creates a loosely defined front, but with random timing of precise moments of failure of individual asperities. This assumption permits one to explain incoherence of HF radiation in the time domain, introduced earlier in (GUSEV 1983) on an abstract level. The model presented here elaborates on this scheme.

In the frequency domain, both in G88 and in B88, the incoherent (“energy”) summation of spectra generated by individual asperities was assumed, resulting in a spectral model with two characteristic corner frequencies and an interval of ω^{-1} trend between them. From an observational viewpoint, this spectral pattern explained the emergence of two characteristic frequencies of an empirical source spectrum of GUSEV (1983) (whose f_2 is essentially f_{c2} of the present paper); it was also supported by the limited analysis of observational data in G88. Recently, GUSEV (2013a) reviewed many empirical studies of strong motion Fourier acceleration spectra and source acceleration spectra. The vast majority of these data indicate that f_{c2} exists at least in the form of low-frequency cutoff of acceleration spectrum. This cutoff practically never matches f_{c1} that is close to inverse rupture duration; very often $f_{c1} \ll f_{c2}$. These facts reliably indicate the reality of the intermediate spectral branch with its slope between 0 and 2; however, this slope may deviate from the accurate value 1.0 (cf. BOATWRIGHT and CHOY 1989).

Both in B88 and G88, the distance R_s over which fault-guided waves propagate was discussed. In B88, this point was treated in more detail, and the special notion of “slip radius” was introduced for R_s . In terms of an estimate, both in B88 and G88 it is assumed that R_s is close to fault radius R_c . Therefore, as seen retrospectively from the spectral patterns constructed below, they could not construct even qualitatively realistic theoretical spectra. To correct this deficiency of the early work is one of the main

aims of the present paper. It will be shown that the value of R_s has a prominent effect on spectral shapes. And specifically when it approaches the fault radius, two-corner spectra and the intermediate ω^{-1} spectral slope tend to *disappear*. For spectral shapes to be realistically two-cornered, one needs R_s much below R_c . Slip-pulse width l is an evident candidate to provide an appropriate distance parameter, and equating $2R_s$ to l is the main idea of the present paper. Note that this assumption is physically plausible: slip pulse is just the place where fault walls are not engaged; in this way, slippage becomes possible, and fault-guided waves are able to propagate.

It should be added for clarity that there are two processes that are deeply interwoven in Case F3: (1) development of dislocation/slip within the slip-pulse strip (that follows from its definition as *slip* pulse) is associated with the *static* component of the fault-guided wavetrain; and (2) formation of *radiated body waves* is caused by the *wave* component of the same wavetrain, when it dies off. Thus, the two phenomena, slip and radiation, are two aspects of the same process.

4. Fault Asperity Theory (Cases F1 and F2) as the Basis of the Present Model

In DK83 (Case F1), an infinite fault is considered formed by frictionless contact of two elastic half-spaces. There is a limited welded patch or “asperity” loaded with shear, and it fails. In the process of failure, the rupture front propagates over the asperity surface; at the moment of arrival of this front to an element of the asperity, local stress drops to its residual value on this element, and stress drop arises. The rupture front generates body waves P and S in each halfspace, and also a fault-guided (Rayleigh, inhomogeneous S and static) wavetrain that propagates along surfaces of the fault. For the SH wave, the displacement and velocity at a far-field receiver, at a point $\mathbf{x} = \{x, y, z\}$ and time t can be written as

$$u^{SH,\infty}(\mathbf{x}, t) = A \int_{\Sigma_a} \tau(\xi) H(t - (R - \xi \cdot \boldsymbol{\gamma})/c_S - t_{fr}(\xi)) dS; \quad (1a)$$

$$A = \frac{\Re_F^{SH}}{4\pi\rho c_S^2 R}$$

$$\dot{u}^{SH,\infty}(\mathbf{x}, t) = A \int_{\Sigma_a} \tau(\xi) \delta(t - (R - \xi \cdot \gamma) / c_S - t_{fr}(\xi)) dS \quad (1b)$$

where Σ_a is the asperity patch, located on a planar fault with its element dS ; the hypocenter is at $\xi = 0$; $R = |\mathbf{x}|$; $\gamma = \mathbf{x}/R$; ρ is density; \mathfrak{R}_F^{SH} is the radiation pattern of SH waves radiated by a point force; $H(\cdot)$ is the unit step and $\delta(\cdot)$ is a delta-function. Similar formulas exist for P and SV waves, with the SV case technically more sophisticated. Note that no waves are generated by parts of the fault outside Σ_a (fault-guided waves generate no far-field body waves). To be accurate, the model permits non-zero, finite friction outside Σ_a ; the crucial property is not the level of cohesion but the lack of displacement-jump-related weakening (sliding friction must be equal to static friction). Therefore, the stress drop equals zero over these parts; henceforth they will be referred to somewhat loosely as “low-cohesion” parts. In this case, qualitatively, the waveform defined by (1a) is a step $H(\cdot)$, convolved with a smoothing window with its width close to T_a . Correspondingly, (1b) is a one-sided, say, positive, pulse with similar duration. See sketch on Fig. 1a, d for illustration. The area of the pulse (1a) equals the final step-like static displacement whose value, as can be derived from (1a), is

$$\begin{aligned} u^{SH,\infty}(\mathbf{x}, \infty) &= \int_{\Sigma_a} \dot{u}^{SH,\infty}(\mathbf{x}, t) dt = A \int_{\Sigma_a} \tau(\xi) dS \\ &\equiv AF_0 \end{aligned} \quad (2)$$

For the average amplitude of positive velocity signal of duration $\approx T_a$, based on (1, 2), one can derive an estimate

$$\dot{u}^{SH,\infty}(\mathbf{x}, t) \approx AF_0 / T_a \quad (3)$$

The $\tau(\xi)$ function that enters the above discussion is

$$\tau(\xi) = \sigma_{dyn}(\xi, t)|_{t=t-failure} - \sigma_f(\xi) \quad (4)$$

where $\sigma_f(\xi)$ is residual friction and $\sigma_{dyn}(\xi, t)$ is the time-dependent stress level, taken at the moment of failure; thus, it can be equated to yield stress $\sigma_y(\xi)$. It is often assumed (e.g. B88; OGLESBY and DAY 2002) that pre-earthquake initial stress $\sigma_0(\xi)$ is closely correlated with $\sigma_y(\xi)$, and local values of $\sigma_0(\xi)$,

being below $\sigma_y(\xi)$ everywhere but at the rupture nucleation point, are still comparable to $\sigma_y(\xi)$. To justify such an assumption, it may be noted that at points ξ where $\sigma_0(\xi)$ is only infinitesimally below $\sigma_y(\xi)$, rupture propagation velocity would be near to or above its critical value (c_S or c_R). Conversely, in the case of a barrier, where $\sigma_0(\xi)$ is significantly below $\sigma_y(\xi)$, the rupture must significantly decelerate (or even stop in the case of an impenetrable barrier). The actual range of observed average rupture velocities, typically 0.65–0.85 c_S , directly indicates that $\sigma_0(\xi)$ is only marginally below $\sigma_y(\xi)$ over most of the fault area. Following OGLESBY and DAY (2002), one can believe that $\sigma_0(\xi)$ values are 1.2–2 times below $\sigma_y(\xi)$. Another argument in support of close correlation of fields of $\sigma_0(\xi)$ and $\sigma_y(\xi)$ follows from the argument of LAY and KANAMORI (1981) who suggested the existence of large-size stress peaks or asperities on the fault plane, created in the course of interseismic fault evolution; their reasoning applies both to $\sigma_0(\xi)$ and $\sigma_y(\xi)$, and may well be valid for asperities of various sizes, not only for large ones. Based on these considerations, random field models, which are used henceforth, are thought to be applicable similarly to $\Delta\sigma(\xi) = \sigma_0(\xi) - \sigma_f(\xi)$ and $\tau(\xi)$.

In the present paper, like (implicitly) in DK83, DK86, $\tau(\xi, t)$ is assumed to drop instantly at the rupture front. This is simplification; generally, it might be more realistic to assume a less abrupt dying-out of cohesion (i.e. its evolution from $\sigma_y(\xi)$ to the “stationary”, low slip rate $\sigma_f(\xi)$ at a point, related to slip-weakening). However, the numerical estimates of the cohesion zone width derived from laboratory, geological and accurate seismological data (see e.g. BEN-ZION and SAMMIS 2003) are very low, much smaller than the cell size of the grid used here, and related stress evolution during failure may be assumed abrupt. There is, however, another possible mechanism for stress drop to develop gradually, with time-dependence of $\sigma_f(\xi)$ related to possible expressed velocity weakening (see e.g. DI TORO *et al.* 2011). In this way, σ_f values may drop down to values significantly below those characteristic for low slip rates; and formation of these low σ_f values, related to accelerated local slip, may take appreciable time. This possibility will be ignored in the following.

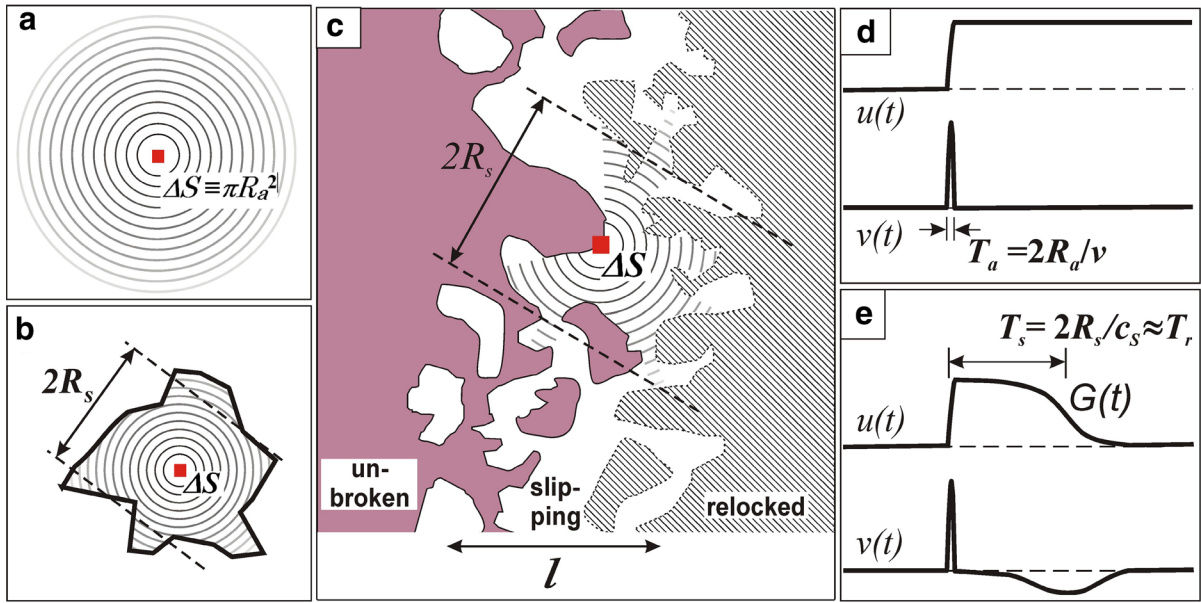


Figure 1

Cartoons of fault-guided (mostly Rayleigh) waves propagating from a single failing fault element ΔS , and of related far-field waveforms. **a** (Case F1)—Rayleigh waves from a fault element ΔS that constitutes a small failing asperity on an unbounded frictionless fault; **b** (Case F2)—same for an asperity located within a limited cohesionless area of size $2R_s$. **c** (Case F3)—as the source of Rayleigh waves, an individual element ΔS of earthquake rupture front is supposed (among many such elements). In **c**, instant positions are shown: of random multiply connected rupture fronts, represented as a boundary (solid tortuous line) between unbroken (grey or pink in color) and slipping (white) areas; and of a healing front with similar geometry, represented as a boundary (dashes) between slipping and locked-in (hatched) areas. The general direction of rupture propagation (i.e. of the front strip or of “macroscopic front”) is from left to the right. The area where Rayleigh waves from ΔS propagate coincides with the “slip patch”, of size $2R_s$, associated with this ΔS . For each particular ΔS , an individual patch of this kind exists. Rayleigh waves can propagate only within the limits of the slipping (white) area; this area is an overlap of slip patches associated with all individual ΔS that constitute the instant position of a rupture front. Surface wave diffraction and tunneling are ignored; the abrupt screening of the wavefield by obstacles shown on the sketch is a simplification only. Looking at the sketch **c**, one should keep in mind that it depicts a snapshot; actually, both fronts are travelling and change their shape; a more adequate picture must be movie-like. **d**—far-field time histories of displacement and velocity for the Case **a** (F1); **e**—same for cases **b** (F2) and **c** (F3)

The model DK83 has been extended in DK86 (Case F2) for an asperity surrounded by a larger low-friction fault region of finite size $2R_c$. In this case, fault-guided waves do not run to infinity, but die away at the boundary of this region, where they are diffracted and converted to body waves. Having arrived at the receiver, these constitute an additional term to the signal (1a). This term is lagged behind by, approximately, T_c , and its sign is opposite to that of (1a), say, negative. At $t \gg T_c$ the contribution of this term to residual body wave displacement precisely compensates (1a). The displacement signal can now be written as:

$$u^{SH}(\mathbf{x}, t) = A \int_{\Sigma_a} \tau(\xi) G(\mathbf{x}, t - [(R - \xi \cdot \boldsymbol{\gamma})/c + t_{fr}(\xi)]) dS \approx A(F_0/T_a)T_c \quad (5)$$

where $G(\mathbf{x}, t)$ is an elementary signal generated by radiator dS at ξ . It is assumed for simplicity that $G(\cdot)$ are the same for all ξ within Σ_a . $G(\mathbf{x}, t)$ is a one-sided, e.g. positive, trapezoid-like pulse, asymmetric, with step-like leading edge and gradually decaying trailing edge:

$$G(\mathbf{x}, t) = H(t) - \int A(\mathbf{x}, s) H(t - s) dS \quad (6)$$

where $A(\mathbf{x}, t)$ is an appropriate unit-area window function, with duration on the order of T_c ; in the case of far field, $A(\mathbf{x}, t)$ can be considered as independent of ξ . In integration (5) the property of positivity, inherent for $G(\mathbf{x}, t)$, is preserved. Thus, displacement pulse $u^{SH}(\mathbf{x}, t)$ is one-sided, as usual in seismology. Its characteristic duration equals (1–2) T_c .

5. Earthquake Source Model (Case F3)

5.1. Running Slip Pulse and “Slip Patch”

Case F2, considered in DK86, is one when fault-guided waves propagate away from a small single asperity. On the basis of DK86 and DK88, and following B88 and G88, one can generalize this case and believe that radiation from an earthquake source of a general kind can be represented again by the same Eq. (5), modified as:

$$u^{SH}(\mathbf{x}, t) = A \int_{\Sigma} \tau(\xi) G(\mathbf{x}, t - [(R - \xi \cdot \gamma)/c + t_{fr}(\xi)]) dS \approx A(F_0/T_a)T_c \quad (5^*)$$

Here, integration is spread from a small patch Σ_a onto the complete fault area Σ , of size $2R_c$. Now let us replace the integral in (5*) by the integral sum over small elements ΔS . Each ΔS , be it strong (an element of a true asperity or an entire such asperity) or weak, now plays the role of a single asperity of DK86 (of size $2R_a$) and is now included in summation. Elements ΔS are assumed to be of comparable size and isometric, and their characteristic size can be written as $\Delta S^{0.5}$.

In a partial analogy with Case F2, let us consider a patch on the fault plane, around ΔS (“slip patch” of B88), that temporarily loses cohesion after rupture passes over ΔS . Within this patch, fault slip is localized associated with stress drop at $\Delta S(\xi)$, and fault-guided waves generated by ΔS have non-zero amplitude. The characteristic size of the slip patch is denoted as $2R_s \gg \Delta S^{0.5}$. Different from with G88 and B88, it is assumed that this size is significantly smaller than the source size: $R_s \ll R_c$. Overall, the following double inequality is assumed true: $\Delta S^{0.5} \ll R_s \ll R_c$. It should be emphasized that for each individual ΔS (each ξ), there is an individual, specific slip patch. Still, the notion of a characteristic or average slip radius is considered meaningful.

A critical further assumption is based on the observation that the conditions of low cohesion around a point ξ are realized just when the running slip pulse crosses its neighborhood. Thus, one can believe that the slip patch size $2R_s$ and the slip-pulse width l of SPM (Fig. 1c) are close to one another.

The assumption $2R_s \approx l$ is the key one here. The relative value of R_s as compared to R_c is a significant model parameter. The denotation $C_H = l/L$ will be used to recall Haskell and Heaton, originators of SPM, and it is assumed here that $R_s/R_c = C_H$. It should be noted that slip patches associated with individual failing fault elements ΔS that constitute the entire instant rupture front overlap to a large degree, and their aggregate (union) is assumed here to constitute the strip instantly occupied by propagating slip pulse.

The shape of the specific $G(\mathbf{x}, t)$ function associated with particular ξ depends on the rupture front configuration and evolution in the vicinity of ξ , on details of propagation and decay of fault-guided waves radiated by $\Delta S = \Delta S(\xi)$, and also on the ray direction γ . To obtain approximate numerical estimates, the dependence of $G(\mathbf{x}, t)$ on ξ and γ is ignored in what follows, and for any ξ , the tentative pulse shape is taken after B88 as:

$$G(\mathbf{x}, t) = G_0(t) = \begin{cases} H(t) - 0.5(1 + \cos \pi t/T_B); & t < T_B \\ 0 & t > T_B \end{cases} \quad (7)$$

Here, T_B is pulse duration, set as $1.667T_r$ to provide the value of the centroid of the pulse (7) to be equal to $0.5T_s = 0.5l/v$. Thus, the distance of complete decay of guided-wave amplitude is set as $1.667l$.

The complete body wave displacement pulse (5, 5*) with its amplitude of the order AF_0T_r/T_c and duration of the order of T_c has its integral close to $AF_0T_r = (A/c_s)F_0 \cdot 2R_s$. As usual, such an integral is related to the seismic moment M_0 of the source. Generalizing the results of DK86, B88 one can write:

$$M_0 \approx F_0 \cdot 2R_s = F_0l. \quad (8)$$

where F_0 is the total seismic force of an earthquake source (see Eq. 2). [Note that F_0 as introduced here is a dynamic entity defined by $\tau(\xi)$, not a static one defined by $\Delta\sigma(\xi)$] For more accurate calculations, one should account for the position of the ΔS patch within source area. In DK86, asperity was positioned at the centre of a circular fault. For asperity (or ΔS patch) located arbitrarily, factor A in (5) depends on the position of asperity within the large source,

and includes an additional coefficient, equal to $2/3$ on the average for the case of circular source (B88). The variation of factor A over the fault area is neglected, and the average coefficient $2/3$ is assumed to be incorporated into the value of factor A .

In DK88, a fault is simulated through multiple local asperities, and waveforms were analyzed that result from their breakdown. It was found that at some points, negative stress drop may appear, but with relatively small, negligible amplitude. Also, for natural earthquakes, there is a possibility of overshoot during the previous event on the same spot of a fault; this again may create limited negative stress drop. Still, the results of DK88 suggest that such effects must be secondary, not so strong as to violate the assumption of non-negativity of the wave displacement pulse (5, 5*). For this reason, the simple assumption of positive $\tau(\xi)$ combined with positive $G_0(t)$ was considered acceptable.

As one can see from DK83, the theory derived above will be valid also for P waves with evident modification of using single-force P radiation pattern. The case of SV waves (polarized in a plane orthogonal to Σ) is more complicated as complex coefficients may arise in this case. This does not significantly affect noise-like HF waveforms. Thus, one can consider the developed approach to be mostly valid for body waves and especially for their amplitude spectra.

5.2. Stress Drop Field

In his stochastic fault model, ANDREWS (1980) assumed that final slip $D(\xi)$ is a self-similar (in a broad sense, or “self-affine”) random function with 2D Fourier spectrum close to $1/k^\alpha$. This behavior can be accurately valid only over an infinite plane. For the case of a source of finite area, low-wavenumber cutoff must be applied; also, for the case of tectonic earthquake, $D(\xi)$ must have positive average. Moreover, both seismogeology and inversions indicate that $D(\xi)$ can be assumed to be positive over entire Σ despite minor deviations found by some inversions. The assumption of self-similarity approximately agrees with the results of inversions of real sources (TSAI 1997; SOMERVILLE *et al.* 1999; MAI and BEROZA 2002). ANDREWS (1980) notes that fields of final slip and

of static stress drop $\Delta\sigma(\xi)$ are rigidly connected. In the wavenumber domain, for an infinite fault, their relationship is close to multiplication by k^1 ; therefore, $\Delta\sigma(k) \propto 1/k^\beta = 1/k^{\alpha-1}$, and similar behavior is further assumed for $\tau(k)$. As a refinement of self-affinity, strict-sense self-similarity [Hurst exponent $H = 1$ for $D(\xi)$] was also proposed and substantiated for real faults by ANDREWS (1980); in such a case $\beta = 1$ (and $\alpha = 2$). Although the analysis of inverted final slip maps does not accurately match the hypothesis that $\alpha = 2$ (and thus $\beta = 1$), the simple assumption that $\beta = 1$ will be used henceforth as the most plausible from general physical considerations. The selection of amplitude spectral shape $\tau(k) \propto 1/k^\beta$ requires power spectrum of $\tau(\xi)$ to behave as $1/k^{2\beta}$; in this way, correlation properties of random field $\tau(\xi)$ are specified.

To perform the simulation, one must also specify the probability law for (positive) local random values of $\tau(\xi)$. The relative scatter of these values (relative with respect to their own mean) is set through coefficient of variation $CV_\tau = (\text{Var}(\tau(\xi)))^{0.5}/E(\tau(\xi))$; as for the distribution law $p(\tau)$, it is assumed lognormal. Note that the particular choice of the lognormal law has no solid basis: one might use, e.g., Weibull or gamma law. What is really significant is the behavior of the tails of $p(\tau)$. Because of (1b) and (5*), these tails can be expected to be related to similar tails of velocity and acceleration amplitude peaks of HF radiation. This important connection should not be thought of as a general one; it is valid in the limited proportion of cases when the distorting effects of path and site are not too strong, and the duration of an accelerogram is not much expanded because of scattering and multipathing (cf. GUSEV 1988, 1996). It also should be kept in mind that the relationship between tails of $p(\tau)$ and those of peak amplitudes is not immediate, as discussed in GUSEV (1992). In the case when tails of the $p(\tau)$ distribution law are sufficiently heavy, they are almost directly reflected in the tails of amplitude peaks. With less expressed tails, this relationship is less close. The question of acceleration peak statistics was recently discussed in GUSEV (2011a, 2013a) in some detail; that discussion implies that the upper tail of the distribution of the observed peak acceleration is only moderately heavy. The use of lognormal law with $CV = 0.7\text{--}1.0$ for acceleration peaks seems to be a

reasonable starting approximation. On a different line, in GUSEV (2011b), the statistics of inverted slip distributions was analyzed, and it was found that the distribution of local final slip can be approximated by the lognormal law with $CV \approx 1.0$ (or by exponential law). Unfortunately, these fragments of information do not match well: one can expect tails of the distribution of acceleration peaks to be relatively enhanced (and corresponding CV value tangibly larger) as compared to peaks of slip distribution. Still, for want of anything better, similar lognormal law, with CV_τ in the range 0.7–1.0 was used for simulation of $\tau(\xi)$. Simulated values of $\tau(\xi)$ are positive, as assumed above. Note that the operator that converts $\tau(\xi)$ to $D(\xi)$ is convolution with positive kernel; therefore, $D(\xi)$ is also a positive function.

5.3. Random Rupture Front and a Technique for its Simulation

The shape of the earthquake rupture front is traditionally thought to be a smooth line. Such a line has a well-defined local normal, and it defines the local direction of rupture propagation. This concept needs to be generalized for the case of a “lacy” random rupture front as introduced here. (Generally, one can imagine random fronts whose realizations are kept smooth, but this degree of randomness is too weak for our purpose). Let us first consider mean (ensemble-average) evolution of a rupture front, and assume the mean front to be again a smooth line with a well-defined normal. In the vicinity of a certain point ξ let us consider the coordinate x' along this normal, with $x' = 0$ at the crossing of the normal with mean front, and let us introduce “front arrival time function” $t_{fr}(x')$. Now consider points of the normal at a certain time moment. The *mean* front forms a crossing at a single point $x' = 0$ as defined; sample *random* fronts will cross the normal at various points around $x' = 0$ forming a probability distribution $p(x')$. It should be emphasized that each single sample “lacy” front will, as a rule, form *many* crossings with the normal. Thus, even a single “lacy” front will occupy a finite interval on the x' axis. When normals are considered for many points of the mean front, these intervals form a finite band along a mean front, or “front strip,” of characteristic width

w . Instead of fixing time moment, one can broaden a viewpoint and consider front arrival time $t_{fr}(x')$ as a function of x' . In the deterministic case, $t_{fr}(x')$ is a one-to-one and monotonous function. In the stochastic case, $t_{fr}(x')$ is, normally, not monotonous, and the inverse function $x'(t_{fr})$ becomes, typically, multiple-valued. As usual, assuming ergodicity, one can believe that mean (ensemble-average) fronts can be estimated (and visualized) as smoothed or low- k -passed versions of sample fronts. Such mean or low-resolution fronts of smooth shape, can be called “macroscopic fronts”, whereas the actual high-resolution lacy shape can be called “microscopic front”.

Complex non-monotonous evolution of fronts is a necessary condition for formation of usually observed incoherence of high-frequency radiation from a source. This consideration is mentioned only very loosely by BOORE and JOYNER (1978) but clearly in DAY *et al.* (2008). Dynamical rupture models with marked contrasts of stress drop show jumps of the front (DAY 1982), meaning multiple-valued $x'(t_{fr})$. Observations (SPUDICH and CRANSWICK 1984; ARCHULETA 1984) reveal qualitatively the same phenomenon. Following GUSEV (2013a), it is assumed further that the rupture front is “lacy”. It is a wiggling line accompanied by “lakes” and “islands”, or a “polyline”; it is multiply connected. After the works of Mandelbrot, it is natural to assume this polyline to have fractal geometry; this assumption also greatly simplifies its simulation. The polyline occupies the “front strip” of width w . It is assumed that w is close to l , and the relationship $w \approx l$ is followed in simulation. At the same time, simulation is organized so that w is close to $2R_s$, this is attained by the proper selection of $T_B = (5/3) T_s$ in (7). To provide these properties, and make the contours of the mean or smoothed front look plausible, the front arrival time (failure time) at ξ is represented as the sum of three terms:

$$t_{fr}(\xi) = Q_{det}(\xi) + Q_{rnd}(\xi) + Q_{lk}(\xi) \quad (9)$$

Here

- (i) $Q_{det}(\xi)$ is deterministic term that describes the systematic behavior of rupture front, simulated as $Q(\xi) = l\xi - \xi_h l/v$ where ξ_h is the hypocenter that represents the vertex of the cone $t = Q_{det}(\xi_1, \xi_2)$. In itself it forms accurately circular mean fronts.

- (ii) $Q_{\text{rnd}}(\xi)$ is a random, stochastic term that provides the geometry of the rupture front that is “lacy” at any time instant, with wiggling shape and fragmented structure. It is a sample of a self-similar random function, is positive, and has a preset spectrum $\propto 1/k^\delta$. The distribution law for local values of $Q_{\text{rnd}}(\xi)$ is selected as Rayleigh law, with twice the mean value equal to $T_w = l/v = T_s = T_r$. Therefore, the microscopic front wiggles within the front strip, of width $w = l$, that trails after the macroscopic front. The trailing edge of this strip constitutes the “macroscopic healing front”. The condition $T_w \approx T_s$ provides the required match between the propagation distance of fault-guided waves and the width of slip-pulse.
- (iii) $Q_{\text{lk}}(\xi)$ is another random, stochastic term of limited amplitude and secondary importance. It has smooth relief, ensured by imposed low- k spectrum. It perturbs unrealistic, primitive circular shapes of mean fronts as generated by $Q_{\text{det}}(\xi)$. It is simulated by the same procedure as used for $Q_{\text{rnd}}(\xi)$, with low- k filter added and a somewhat modified set of other parameters.

Overall, a smoothly propagating “macroscopic” front is formed by the sum of $Q_{\text{det}}(\xi)$ and $Q_{\text{lk}}(\xi)$, whereas $Q_{\text{rnd}}(\xi)$ is a perturbation term that provides fine “microscopic” details.

The described procedure has certain weakness. The value of l (and thus T_w) was implicitly assumed as fixed during front propagation. The assumption of a fixed l value makes relative front perturbation overly strong at the early stages of rupture growth, when instant rupture size is comparable or even lower than w and/or l . To amend this deficiency, T_w (and implicitly T_r) is made time dependent: $T_w(\xi) \propto Q_{\text{det}}(\xi)^\eta$. The preset T_w value discussed above is considered as an average value over entire fault, and used to properly scale the $T_w(\xi)$ function.

6. Simulation and Its Results

The developed numerical procedure includes the following steps (the accepted parameter values are given in parentheses):

- (a) selecting: the size of a rectangular source ($L \times W = 38 \times 19$ km, corresponds approximately to the magnitude range $M = 6.8\text{--}6.9$), time step dt (0.013 s), distance step dx (0.037 km); v (3.0 km/s); c_s (3.5 km/s); hypocenter position ξ_h ($\xi_1 = 0.12L$, $\xi_2 = 0.24W$);
- (b) setting control parameters: $\beta(1.0)$, C_H , (0.0075 \div 0.24), CV_τ (0.8), $\eta(0.5)$ and $\delta(1.2)$; the shortest wavelength for $Q_{\text{lk}}(\xi)$ is set close to 1.5 km.
- (c) generation of random fields $t_{\text{fr}}(\xi)$ and $\tau(\xi)$ (Fig. 2);
- (d) calculation of $u^{SH}(\xi, t) \equiv u(t)$ through (5*, 6, 7) (Fig. 3a) and of its amplitude spectrum $u(f)$;
- (e) determination of normalized displacement amplitude spectrum $u_n(f) \equiv u(f)/u(f)|_{f=0}$ and of associated acceleration spectrum $\ddot{u}_n(f)$ (Fig. 3b).

The discussed modeling procedure is entirely kinematic, and no connection is assumed between $t_{\text{fr}}(\xi)$ and $\tau(\xi)$. For plotting, all simulated spectra are smoothed at moderate-to-high frequencies using log-equal bins (three bins per octave). Spectra are normalized by displacement pulse area $u(f)|_{f=0}$ (i.e.

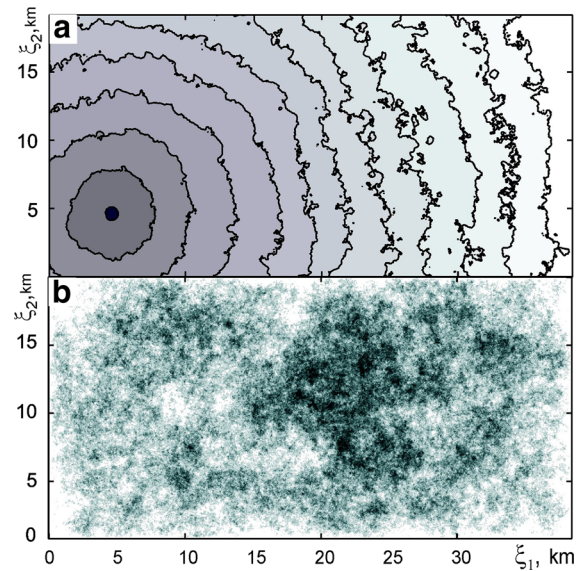


Figure 2

a Propagating rupture front of a sample simulated source. Positions of the front, i.e. isolines of the sample $t_{\text{fr}}(\xi)$ function, are plotted each 0.89 s. Shades of gray code time: the later, the lighter. Black dot is the nucleation point. **b** Sample random field $\tau(x, y)$ with $1/k$ mean amplitude spectrum; shading reflects amplitude; maxima are darker

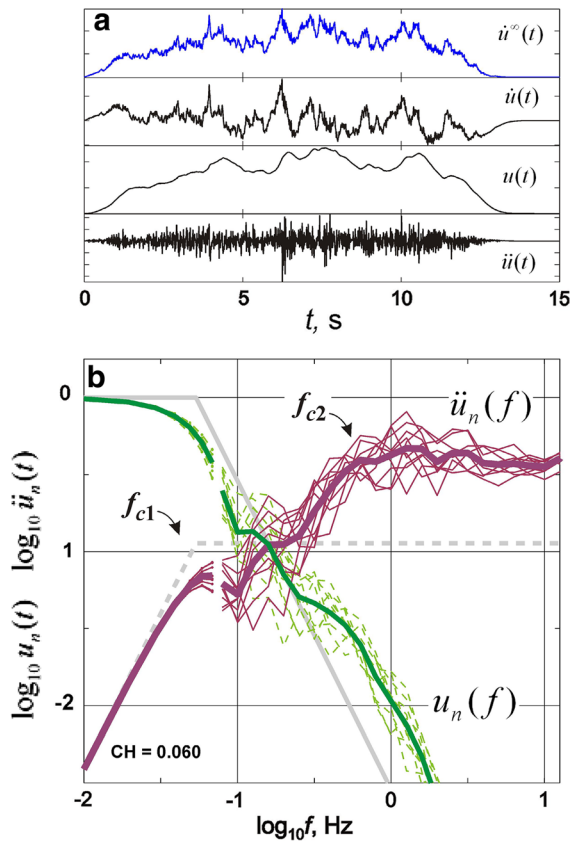


Figure 3

Typical results of simulation. **a**—Signals $u^\infty(t)$, $\dot{u}(t)$, $u(t)$ and $\ddot{u}(t)$ at the receiver. Amplitude scale is arbitrary. **b**—Normalized spectra $\ddot{u}_n(f)$ (dashes) and $u_n(f)$ (solid line), raw (on the left, at lower f) and smoothed (on the right). Thin lines: ten individual spectra; thick curve: their average. In this and further pictures, gray angular shapes on the background are schematic spectra of the common ω^{-2} model; their corner frequency f_{c1} is set equal to $1/2\pi T_{rms}$, where T_{rms}^2 is the average second normalized central power moment for $u(t)$ (SILVER 1983). Gap in a spectral curve on this and next figures indicates switching from raw to smoothed spectra

always setting M_0 value to unity). This allows one to cancel all parameters involved in A , and to concentrate on shapes and relative levels of spectra that are of main interest in the present study. The lower (common) corner frequency f_{c1} of simulated spectra is essentially constant as it is mostly defined by L , ξ_h , and v , all of them fixed. This means that not only magnitude, but also global stress drop of simulated sources is fixed.

Simulated signals $u(t)$, $\dot{u}(t)$ and $\ddot{u}(t)$ (Fig. 3a) qualitatively agree with those observed in real earthquakes at moderate distances from a fault. (No attempt is made here to imitate records obtained close to a fault.) The average smoothed acceleration

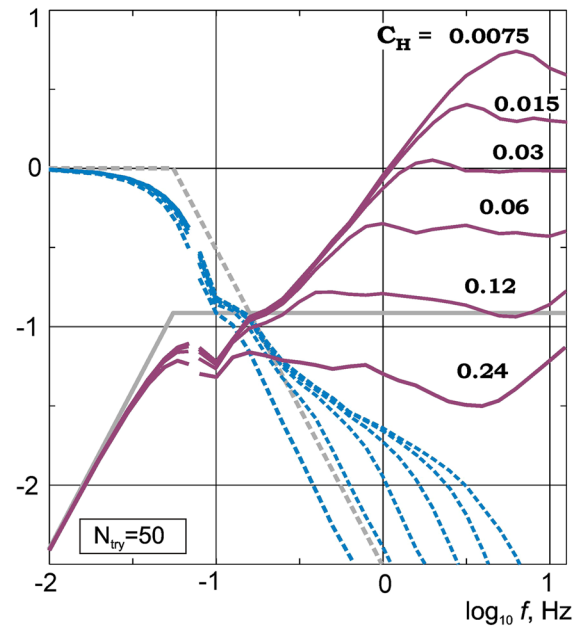


Figure 4

Normalized simulated spectra $\ddot{u}_n(f)$ (solid lines, purple online), and $u_n(f)$ (solid blue online, dashes on paper), averaged over 50 realizations, for a set of values of relative slip-pulse width C_H , at fixed values of other parameters

spectrum (Fig. 3b) is flat, and clearly shows the second corner-frequency f_{c2} . Both these features also qualitatively agree well with observations, and moreover with the ω^{-2} model, in its two-corner ($\varepsilon < 1$) version after BRUNE (1970).

The parameter that controls the shape of the acceleration spectrum most significantly is C_H ; it affects both the relative level of acceleration spectrum and the position and degree of expression of the f_{c2} corner. Its role is seen in Fig. 4: the f_{c2} corner is manifest clearly when $C_H \leq 0.12$. At larger C_H it disappears, and a simple ω^{-2} shape with no distinct f_{c2} corner can be expected at C_H about 0.15–0.20. Let us denote actual flat acceleration spectral level as A_{HF} , and its value for the primitive ω^{-2} shape of the case $f_{c1} = f_{c2}$ (grey dashes on Fig. 3) as A_{1HF} . The following approximate relationships hold

$$f_{c2}/f_{c1} \approx 0.67/C_H \quad (10)$$

$$A_{HF}/A_{1HF} \approx 0.17/C_H \quad (11)$$

The most significant fact here is that of approximate inverse proportionality. The numerical factors are interesting; however, they are not of general

validity, and may depend, e.g., on the aspect ratio of the fault, or on the selection of the CV_τ parameter. Between f_{c1} and f_{c2} the acceleration spectral shape can have a $f^{1.0}$ segment but on the whole deviates from a simple $f^{1.0}$ line connecting two corners; it shows certain concavity in the range $(1-1.4)f_{c1}$.

The simulation results were tentatively checked against real spectra using the well-established empirical spectral model of HALLDORSSON and PAPA-GEORGIOU (2005) for the interplate data set. From Fourier spectral shapes expected from their spectral family at $M_w = 6.8$ one can crudely estimate the parameters f_{c2}/f_{c1} and A_{HF}/A_{1HF} ; their values are about 7 and 4, correspondingly. From (10) and (11) one can obtain from these numbers the estimates for C_H equal to 0.1 and 0.04, correspondingly. Their average value is 0.07, quite comparable with original HEATON'S (1990) estimate of 0.1.

7. Frequency-Dependent Directivity and Incoherence

It was interesting to analyze directivity features of the described model and, particularly, frequency dependence of directivity. Two aspects of directivity are angular dependence of spectral amplitudes, and that of characteristic frequencies (Doppler effect). The numerical procedure that followed Eqs. 5-7 was performed for the fixed $C_H = 0.06$, $v/c_S = 0.85$ and for a set of angles θ between (1) the rupture propagation direction, taken as the positive direction of the ξ_1 axis (abscissa on Fig. 2), and (2) the direction of the receiver ray; these two angles define the γ vector in (5). The y component of the ray vector equals zero. The following set of θ was used: $\theta = 0, 45, 90, 135, 180^\circ$. Average spectra were calculated over 50 simulation runs (Fig. 5); they show the following features (numerical estimates are specific for the selected v/c_S and C_H but qualitative conclusions seem to be of wider applicability):

1. In the frequency band around $f_{c1,90}$ and up to approximately $f_{c2,90}$, both mentioned angular dependencies—for spectral levels as well as for the f_{c1} value—are clearly seen, in a close match to the textbook behavior of deterministic unilateral

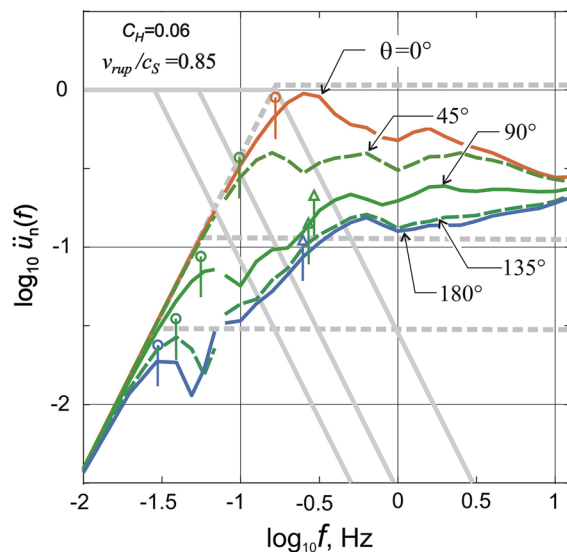


Figure 5
Angular dependence of normalized acceleration spectrum $\ddot{u}_n(f)$ obtained by averaging over 50 simulated sample sources with size, geometry and hypocenter as shown in Fig. 2, with approximate magnitude $M_w = 6.8-6.9$. Five spectra are plotted for angles $\theta = 0$ (forward), 45, 90, 135 and 180° (backward) between the ξ_1 axis and the ray to the receiver. Fault parameters: $C_H = 0.06$, $CV_\tau = 0.8$, $\delta = 1.2$. The gap in the curve indicates switching from raw to smoothed spectra. Spoon-like symbols indicate f_{c1} positions. They were determined via T_{rms} as explained in the caption of Fig. 3. Arrow-like symbols indicate approximate f_{c2} positions, where discernible

fault models. The value of f_{c1} varies from 0.027 to 0.18 Hz, broadly deviating up and down from $f_{c1,90} = 0.055$ Hz.

2. In the discussed band, the contrast of spectral amplitudes is at its maximum (up to ten times) at $f \approx 3f_{c1,90}$; above $f = f_{c2} \approx 5 f_{c1,90} \approx 0.27$ Hz, the contrast diminishes, down to about three times at 3 Hz, and almost disappears at 10-15 Hz.
3. No clear variation of f_{c2} with θ can be noticed.
4. Taking $f_{c2,90}$ as the reference, the critical frequency f_{ucoh} where the transition from LF enhanced to HF diminished directivity takes place is $f_{ucoh} \approx (1-2)f_{c2}$. This critical frequency can be understood as a change from mostly coherent to mostly incoherent behavior of the radiator. The general correspondence between f_{ucoh} , f_{c2} and $1/T_r$ has already been proposed in GUSEV (2013a), see also BERNARD and HERRERO (1994).

SOMERVILLE *et al.* (1997) analyzed frequency dependence of directivity for vicinity of a fault, but

their qualitative results can be expected to be approximately valid also for larger distances. Their analysis sets the just defined transition frequency f_{ucoh} at about 1.5–2 Hz. This value is in approximate agreement with the transition from high to low amplitude contrast that, according to simulation (Fig. 5), takes place within the frequency band 0.4–3 Hz. Although the analysis of SOMERVILLE *et al.* (1997) was performed in bulk for many earthquakes with various magnitudes, our approximate magnitude range $M = 6.7$ – 6.9 (based on the value of the fault area) generally agrees with the dominant range of magnitudes studied in SOMERVILLE (1997). Still, the degree of HF reduction of directivity attained in the present model seems to be somewhat weaker as compared to empirical directivity studies.

8. Discussion

BOORE and JOYNER (1978) and JOYNER (1991) tried to analyze HF radiation on the basis of the notion that one can describe incoherency through non-uniform, random 2D slip rate, and/or non-uniform, random local rupture velocity. However, directivity produced by such a model is unrealistically high; the reason is that phase shifts created by such randomization are insufficient to create mutual cancellation of amplitudes which is required to provide “energy-style” summation of contributions of fault spots, in place of “amplitude-style” summation. See GUSEV (2013a) for further discussion. Random phasing of pulses from fault spots (GUSEV 1983) is a critical condition to provide realistically low directivity. The present model seemingly needs adjustment in order to provide a greater, more realistic degree of reduction of directivity at HF; this means, simultaneously, less degree of coherency.

Some researchers proposed locally random orientation of an instant, local rupture velocity vector within small fault patches (KOYAMA and IZUTANI 1990; BERNARD and HERRERO 1994). Similarly, random omnidirectional orientation of an instant, local rupture front is assumed in DAY *et al.* (2008). This view contradicts in no way the model presented here. Just the opposite; it is easy to see that in a “microscopic”, small-scale view, the “lacy” rupture front assumed

here is indeed, to a large degree, omnidirectional. A close examination of the example case in Fig. 2a shows quite irregular orientation of local normal to the instant rupture front, created by its various wiggles, “islands” and “lakes”. It should be noted that in the present model, there is a definite mean (“macroscopic”) direction of propagation of rupture front/front strip; this systematic behavior must result in certain correlation between arrival times of the mentioned elementary pulses. The obtained numerical results show that the postulated “lacy” structure significantly reduces possible directivity related to such a correlation. Experiments (not shown here) show that in the case of the rupture front of zero width, but with $G_0(t)$ pulse of finite duration, no directivity reduction takes place at arbitrary high frequency.

In addition to significant general reduction of directivity, BERNARD and HERRERO (1994) found the secondary effect of a residual $\cos 2\theta$ directivity with enhanced 0° and 180° directions, and reduced 90° direction (see their Fig. 7a, b). The present model does not support this prediction.

GUSEV (2011a) proposed a strong-motion simulation procedure that features lack of directivity for sufficiently high frequencies; the analog of f_{ucoh} was set (ad hoc) at $7.7f_{c1}$. At higher frequencies, point subsources of the source model of GUSEV (2011a) have no intrinsic directivity. Time histories of these subsources are simulated as uncorrelated, thus their relative phases are random and coherence in this frequency range is suppressed. Alternatively, frequency-dependent coherence can be imposed, with correlation radius proportional to wavelength (GUSEV 1983). Generally, partial coherence amplifies a signal at a receiver as compared to complete incoherence. This model may be used to clarify the question whether frequency-dependent coherence may affect directivity by itself, without any effects related to details of rupture front evolution. This research may be interesting.

There is a significant inter-event scatter among strong-motion parameters, estimated as an inter-event component of scatter of observed strong-motion amplitudes with respect to their mean trends described by GMPE for a given M_0 and distance. From the viewpoint of the present model, such a scatter of

amplitudes has multiple causes, including the variability of at least the following parameters: (1) average rupture velocity v ; (2) global stress drop τ_{gl} , not discussed here, on the order of M_0/LW^2 ; (3) rms local stress drop $\sigma_\tau = CV_\tau\tau_{gl}$, (4) relative slip-pulse width C_H . All these parameters must contribute to inter-event scatter, as well as to also very interesting inter-regional scatter, but the presented results do not permit us to isolate the most relevant parameter or parameters. My opinion is that parameters 2 and 4 are the most significant, but this statement has no solid basis.

From a tectonophysical point of view, the hypothesis of lacy rupture front is the only natural one. As noted in G88, corrugated or rough geometry of fault walls dictates spotty contact between them (or at least heavy-tailed distribution law for fault strength). With an increasing amount of data regarding complex geometry of faults and of instant rupture fronts, the idea of a smooth, simple, “Euclidean” shape of rupture front becomes less and less plausible.

9. Conclusion

The developed “doubly stochastic source model” provides a workable broadband description of earthquake source radiation. It is based on transparent concepts, most of which are not new. A fresh idea is one of a “lacy” fractal rupture front (GUSEV 2013a), an almost inevitable assumption when considering the impossibility to suppress effectively HF directivity in another way. The only really new but critical idea is to relate the size of a slipping patch around an element of the fault plane with the width of propagating slip pulse.

The proposed model permitted us to emulate two well-established features of source spectra: the almost ubiquitous “omega-square” HF branch, and often-observed two-corner spectra. Formation of the second spectral corner, as proposed by a few researchers, is associated, on a conceptual level, with existence of a narrow slip pulse. The particular mechanism for this connection is proposed, and a particular tentative relationship between the slip-pulse width and spectral corner is found.

The simulation suggests that slip-pulse width controls not only the position of the second spectral corner, but also the amplitude level of acceleration spectrum. This relationship, revealed by numerical simulation, may provide at least a partial explanation of the scatter of HF ground motion amplitudes at a certain particular set of values of magnitude, global stress drop and v/c_S (Mach number w.r.t S waves). This conclusion may be important for earthquake hazard applications. In addition, it might be interesting to apply an empirical check to the model prediction (that directly follows from Eqs. 10 and 11) that the values of second corner frequency and acceleration spectral level must be positively correlated.

The range of values of the slip-pulse width to fault length ratio C_H needed to generate realistic spectral shapes, of approximately 3–15 %, matches well with the original estimates of HEATON (1990) based on radically different information. At high values of C_H , the model generates single-corner spectra. Therefore, observations of single-corner, clearly double-corner or intermediately shaped spectra in real earthquakes can be associated with the natural variations of the C_H parameter.

The developed model manifests frequency-dependent directivity, with high low-frequency directivity in accordance with common deterministic fault models, and diminished high-frequency directivity that reflects partial incoherence of the source for this frequency range. An estimate is obtained for the critical frequency f_{ucoh} where the transition between these regimes takes place; this estimate matches observations reasonably.

Acknowledgments

Discussions with V.I. Osaulenko and G.M. Molchan were highly valuable. Comments of anonymous reviewers and of the Invited Editor helped to improve the manuscript.

REFERENCES

- AKI, K. (1967). *Scaling law of seismic spectrum*. J. Geophys. Res., 72, 1217–1231.

- ANDREWS, D. J. (1980). *A stochastic fault model. I. Static Case*. J. Geophys. Res., 78, p. 3867–3877.
- ARCHULETA, R. J. (1984) *A faulting model for the 1979 Imperial Valley earthquake*. J. Geophys. Res. 89, 559–4585.
- BEN-ZION, Y., and SAMMIS, C.G. (2003) *Characterization of Fault Zones* Pure Appl. Geophys. 160, 677–715.
- BERESNEV, I., and G. ATKINSON (2002). *Source parameters of earthquakes in eastern and western North America based on finite-fault modeling*, Bull. Seism. Soc. Amer. 92, 695–710.
- BERNARD, P. and A. HERRERO (1994): *Slip heterogeneity, body-wave spectra, and directivity of earthquake ruptures*, Ann. Geofis., XXXVII (6), 1679–1690.
- BOATWRIGHT, J. (1982) *A dynamic model for far-field acceleration*. Bull. Seismol. Soc. Amer. 72 1049–1068.
- BOATWRIGHT, J. (1988) *The seismic radiation from composite models of faulting*, Bull. Seism. Soc. Am, 78, 489–508.
- BOATWRIGHT, J. (2007) *The persistence of directivity in small earthquakes*. Bull. Seism. Soc. Amer. 97, 1850–1861, doi:10.1785/0120050228.
- BOATWRIGHT, J. and CHOY, G.L. (1989) *Acceleration spectra for subduction-zone earthquakes*. J. Geophys. Res, 94, 15541–15553.
- BOORE, D. M. and W. B. JOYNER (1978). *The influence of rupture incoherence on seismic directivity*, Bull. Seism. Soc. Am. 68, 283–300.
- BRUNE, J. (1970). *Tectonic stress and the spectra of seismic shear waves from earthquakes*, J. Geophys. Res. 75, 4997–5009.
- DAS, S., and B.V. KOSTROV. (1983). *Breaking of a single asperity: rupture process and seismic radiation*, J. Geophys. Res, 88, 4277–4288.
- DAS, S., and B.V. KOSTROV. (1986). *Fracture of a single asperity on a finite fault: a model for weak earthquakes?* In: Earthquake Source Mechanics. Washington, Am. Geophys. Union. 91–96.
- DAS, S., and KOSTROV, B. V. (1988), *An investigation of the complexity of the earthquake source time function using dynamic faulting models*, J. Geophys Res, 93(B7), 8035–8050.
- DAY, S. (1982). *Three dimensional simulation of spontaneous rupture: The effect of non-uniform pre-stress*. Bull. Seismol. Soc. Am., 72, 1881–1902.
- DAY, S. M., GONZALEZ, S. H., ANOOSHEHPOOR, R., and BRUNE, J. N. (2008), *Scale-model and numerical simulations of near-fault seismic directivity*, Bull Seismol Soc Am, 98, 1186–1206. doi:10.1785/0120070190.
- DI TORO, G., R. HAN, T. HIROSE, N. DE PAOLA, S. NIELSEN, K. MIZOGUCHI, F. FERRI, M. COCCO, & T. SHIMAMOTO (2011) *Fault lubrication during earthquakes*, Nature, 471, 494–98, doi:10.1038/nature09838.
- GUSEV, A. A. (1983). *Descriptive statistical model of earthquake source radiation and its application to an estimation of short-period strong motion*, Geophys J R Astr Soc, 74, 787–808.
- GUSEV, A. A. (1988). *A model of earthquake source with multitude of asperities*. Vulkanol. Seismol, #1, 41–55 (in Russian).
- GUSEV, A.A. (1989). *Multiasperity fault model and the nature of short-period subsources*, Pure Appl. Geophys, 130, 635–660.
- GUSEV, A.A. (1992) *On relations between asperity population and earthquake population on a fault*. Tectonophysics, 211, 85–98.
- GUSEV, A.A. (1996) *Peak factors of Mexican accelerograms: evidence of non-Gaussian amplitude distribution*. J. Geophys. Res. 101, 20083–20090.
- GUSEV, A.A. (2011a) *Broadband kinematic stochastic simulation of an earthquake source: a refined procedure for application in seismic hazard studies*. Pure Appl. Geophys. 168, 155–200. doi:10.1007/s00024-010-0156-3.
- GUSEV, A.A. (2011b) *Statistics of the Values of a Normalized Slip in the Points of an Earthquake Fault*. Izvestiya, Physics of the Solid Earth, 47, 176–185. [Original Russian Text: Fizika Zemli, 2011, No. 3, 24–33].
- GUSEV, A.A. (2013a) *High-frequency radiation from an earthquake fault: a review and a hypothesis of fractal rupture front geometry*. Pure Appl. Geophys. 170, 65–93. doi:10.1007/s00024-012-0455-y.
- GUSEV, A.A. (2013b) *Fractal earthquake source with slip zone generates acceleration time histories with flat spectra*. Doklady Earth Sciences, Vol. 448, Part 2, pp. 211–213. [original in Russian: DAN, 2013, 448, 465–467].
- GUSEV, A.A., and I.R. ABYBAKIROV. (1996). *Simulated envelopes of non-isotropically scattered body waves as compared to observed ones: another manifestation of fractal heterogeneity*, Geophys. J. Int. 127: 49–60, 1996.
- HALLDORSSON, B., and PAPAGEORGIOU, A. S. (2005) *Calibration of the specific barrier model to earthquakes of different tectonic regions*, Bull Seism Soc Am, 95, 1276–1300. doi:10.1785/0120040157.
- HANKS, T. C., and R. K. MCGUIRE. (1981). *The character of high frequency strong ground motion*, Bull Seism. Soc Am, 71, 2071–2095.
- HASKELL, N. A. (1964). *Total energy and energy spectral density of elastic wave radiation from propagating faults*, Bull Seismol Soc Amer, 54, 1811–1841.
- HASKELL, N. A., (1966), *Total energy and energy spectral density of elastic wave radiation from propagating faults. II. A stochastic fault model*. Bull Seism Soc Am, 56, 125–140.
- HEATON, T. H., (1990). *Evidence for and implications of self-healing pulses of slip in earthquake rupture*, Phys. Earth Planet. Inter., 64, 1–20.
- HERRERO, A., and P. BERNARD, (1994). *A kinematic self-similar rupture process for earthquakes*, Bull Seism. Soc Am, 84, 1216–1228.
- KOSTROV, B. V. (1975). *Mechanics of the source of a tectonic earthquake*. (Nauka Moscow) (in Russian).
- KOYAMA, J., IZUTANI, Y. (1990) *Seismic excitation and directivity of short-period body waves from a stochastic fault model*. Tectonophysics, 175, 67–79.
- LAY, T. and H. KANAMORI (1981). *An asperity model of large earthquake sequences*, in: *Earthquake Prediction—An International Review*, Maurice Ewing Series, vol. 4, D. Simpson and P.G. Richards, Editors; AGU, Washington D.C, pp 579–592.
- MAI, P.M., and G.C. BEROZA (2002). *A spatial random-field model to characterize complexity in earthquake slip*, J. Geophys. Res., Vol. 107 (B11), 2308, doi:10.1029/2001JB000588.
- OGLESBY, D.D. and S. M. DAY (2002) *Stochastic fault stress: implications for fault dynamics and ground motion*. Bull. Seismol. Soc. Amer 92, 3006–3021.
- PAPAGEORGIOU, A. S., and K. AKI, (1983). *A specific barrier model for the quantitative description of inhomogeneous faulting and the prediction of the strong ground motion, I: Description of the model*, Bull Seism. Soc Am, 73, 693–722.
- SHEARER, P.M. (1999) *Introduction to Seismology*, Cambridge University Press, 260 pp.
- SILVER, P. (1983) *Retrieval of source-extent parameters and the interpretation of corner frequency*. Bull. Seismol. Soc. Amer., 73,#6A, 1499–1511.

- SOMERVILLE, P. G., N. F. SMITH, R.W. GRAVES, and N. A. ABRAHAMSON (1997). *Modification of empirical strong ground motion attenuation relations to include the amplitude and duration effects of rupture directivity*, *Seismol. Res. Lett.* 68, 199–222.
- SOMERVILLE, P., K. IRIKURA, R. GRAVES, S. SAWADA, D. WALD, N. ABRAHAMSON, Y. IWASAKI, T. KAGAWA, N. SMITH, and A. KOWADA (1999). *Characterizing crustal earthquake slip models for the prediction of strong motion*, *Seism. Res. Lett.* 70, 59–80.
- SPUDICH, P. and E. CRANSWICK, (1984) *Direct observation of rupture propagation during the 1979 Imperial Valley earthquake using a short baseline accelerometer array*. *Bull. Seismol. Soc. Amer.* 74, 2083–2114.
- TSAI, C. -C. P. (1997). *Ground motion modeling for seismic hazard analysis in the near-source regime: an asperity model*, *Pure Appl. Geophys.* 149, 265–297.

(Received April 13, 2013, revised December 12, 2013, accepted December 19, 2013, Published online February 11, 2014)